

# Compact Ridge Waveguide Gysel Combiners for High-Power Applications

Mohamed M. Fahmi<sup>1</sup>, Jorge A. Ruiz-Cruz<sup>2</sup>, *Senior Member, IEEE*, and Raafat R. Mansour, *Fellow, IEEE*

**Abstract**—This paper presents, to the best of the authors' knowledge, the first realizations of the Gysel-type power combiner/divider in ridge waveguide technology with two different configurations. Gysel combiners exhibit wider bandwidths than traditional combiners, while offering compact designs when implemented in ridge waveguide, compared with traditional waveguide combiners. In addition, Gysel combiners provide relaxed requirements on the power handling capability of the terminating loads in the case of fault conditions, which may result from imbalance between different inputs. The ridge waveguide designs offer better power handling capabilities, especially in comparison with planar designs. These advantages are shown with two different realizations, in top-bottom and side-by-side configurations, exhibiting very wide bandwidths while occupying very compact volumes. These two designs have been simulated, fabricated, and tested. Excellent test results have been obtained, confirming the validity of the concept.

**Index Terms**—Combiner, coupler, divider, power amplifiers, ridge waveguide, wideband Gysel.

## I. INTRODUCTION

RECENT breakthroughs in the solid-state device manufacturing technology resulted in power modules with very high-power levels that are used in very diverse applications, such as wireless communications, space, and ground-based satellite systems, and a variety of radar systems. For instance, high-power radar transmitter development necessitates the efficient combining of many solid-state modules, to arrive at the very high-power levels needed. In addition to high power, these applications often require high efficiency, low noise, and high linearity. The power combiners are key elements [1], [2] of these modules. Power combining techniques have attracted considerable attention over a considerably long period of time and spanning diverse fields [3]–[9], demonstrating the need for power combiners/dividers with high performance.

Some of the recently reported combiner realizations include radial combiners [10]–[14] and junction-based

Manuscript received August 30, 2018; revised November 1, 2018; accepted November 14, 2018. This paper is an expanded version from the 2018 International Microwave Symposium, Philadelphia, PA, USA, June 10–15, 2018. (Corresponding author: Mohamed M. Fahmi.)

M. M. Fahmi is with Defence Research and Development Canada, Ottawa, ON K1A 0Z4, Canada (e-mail: mmfahmi@gmail.com).

J. A. Ruiz-Cruz is with Escuela Politécnica Superior, Universidad Autónoma de Madrid, 28049 Madrid, Spain (e-mail: jorge.ruizcruz@uam.es).

R. R. Mansour is with the Department of Electrical and Computer Engineering, University of Waterloo, Waterloo, ON N2L 3G1, Canada (e-mail: rrmansour@uwaterloo.ca).

Color versions of one or more of the figures in this paper are available online at <http://ieeexplore.ieee.org>.

Digital Object Identifier 10.1109/TMTT.2018.2885521

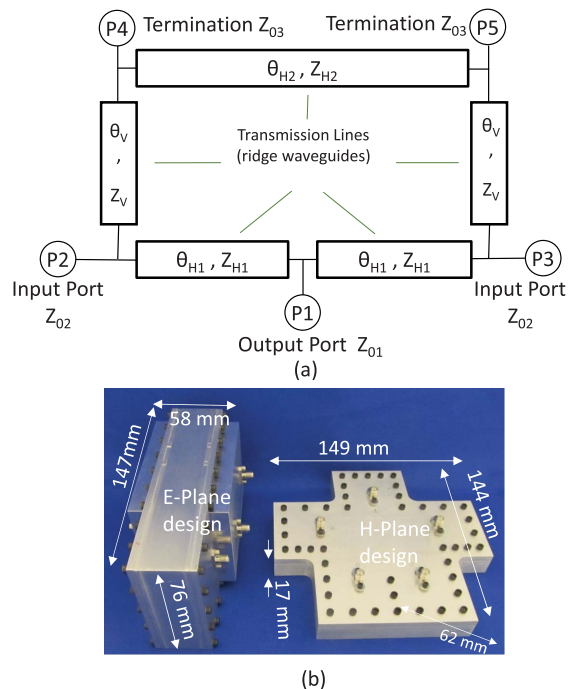


Fig. 1. (a) Generalized ideal circuit model of Gysel power combiner, with the typical use of the ports. (b) Ridge waveguide realizations presented in this paper with integrated coaxial transitions at the C-band.

combiners [15]–[17]. Due to their limited port-to-port isolation, which is directly proportional to the number of input ports, they usually work well for only a large number of inputs. However, under failure conditions for one input, the other inputs will be subjected to reflected power, which necessitates the inclusion of isolators for the protection of individual power modules. This introduces losses, added volume, and nonlinearities to the system.

Classic combining schemes [1] solve this problem by utilizing couplers with high isolation between input ports and with loads attached to the fourth isolated port to handle the diverted power at fault conditions. Examples for such couplers include Riblet couplers as well as magic-T structures [9]. While these diverse couplers can handle high-power levels, they have a limited bandwidth. Moreover, at lower frequencies such as S- and C-band, they are prohibitively large in physical size.

On the other hand, Gysel-type combiners [18], whose basic ideal circuit model is shown in Fig. 1(a), offer a solution that has a wider bandwidth compared to conventional combiners, along with two terminating loads rather than a single

TABLE I  
POWER COMBINER COMPARATIVE PERFORMANCE

Type	Trade-Off
Radial Combiners	Use of one circulator and load per input for protection. Introduction of non-linearity, increased size.
Reactive Junction Combiners	Use of one circulator and load per input for protection. Introduction of non-linearity, increased size.
Riblet coupler-based Combiner	Use of one load per two-way combiner attached at the isolated port, which must handle 50% of the input power.
Magic-T-based Combiners	Use of one load per two-way combiner attached at the isolated port, which must handle 50% of the input power.
Gysel based Combiners	Use of two load per two-way combiner attached at the isolated ports, each must handle 25% of the input power.

terminating load at the isolated ports. Table I summarizes the performance comparison among different power combining schemes. It is worth noting that the rating of the loads attached whether to the isolators, or to the isolated ports in high-isolation couplers, is of prime practical importance. Utilizing Riblet couplers or magic-T requires having loads that are able to handle 50% of the input power, while for the Gysel combiner case, there are two loads that need only to handle 25% of the power each. Usually, two loads rated at 25% can be smaller in size and lower in cost than one load rated at 50%.

Recent realizations of Gysel combiners include mainly microstrip realizations [19]–[23] but also realizations in substrate integrated waveguide and low-temperature cofired ceramics [24], [25] have been reported. Such designs are compact in size, but their power handling capability is relatively low, limiting their use to low-power combining network applications. In comparison with other types of combiners/dividers, the literature in Gysel combiners is less profuse and there is an apparent lack of reported realizations of Gysel combiners in metallic waveguides, which offer the advantages of low insertion losses and high-power handling capability. This paper will, thus, focus on the topic of using ridge waveguides for the Gysel combiner realizations.

Novel ridge waveguide Gysel combiners were first reported in [26] with an initial realization in side-by-side arrangement of the ridge waveguides, which will be referred to as the *H*-plane implementation. The initial work in [26] is extended in this paper by generalizing the design methodology of Gysel combiners in different configurations and topologies, where compactness and suitable manufacturability are prime considerations. An additional implementation will be introduced to provide better power handling, by placing the ridge waveguides on the top of each other, which will be referred to as the *E*-plane implementation. These designs (see Fig. 1(b) for a photograph of the realized prototypes) provide a very good tradeoff between compactness and higher power handling in comparison with planar designs. To the best of the authors' knowledge, these ridge waveguide realizations of Gysel combiners had not been reported previously elsewhere.

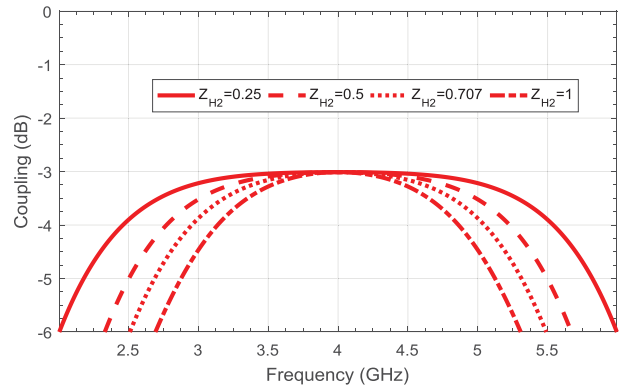


Fig. 2. Variation of the coupling bandwidth for different values of the characteristic impedance  $Z_{H2}$ , normalized to  $Z_0$ , of the transmission line in Fig. 1(a). Other values as in (1).

## II. THEORETICAL NETWORK ANALYSIS

The presented realizations of the Gysel combiner are based on the ideal circuit model shown in Fig. 1(a), or its dual circuit, later on implemented in different ways. The first step in the design process is to synthesize the ideal circuit elements and derive their optimum values.

### A. Ideal Circuit Synthesis

The parameters of the generalized ideal circuit model representing the Gysel combiner are presented in Fig. 1(a). In classical realizations of Gysel combiners [18], the reference impedances of the five ports ( $Z_{01}$ ,  $Z_{02}$ , and  $Z_{03}$ ) are kept at the same level. The electrical lengths of the transmission line branches are set to  $90^\circ$  for  $\theta_{V1}$  and  $\theta_{H1}$ , and to  $180^\circ$  for  $\theta_{H2}$ , at the center frequency. The impedance levels of the transmission line branches are subsequently used to achieve the required electrical performance characteristics such as arbitrary power ratio, return loss level, and port-to-port isolation level [20], [27].

For the presented designs, a 3-dB coupling at the center frequency of the combiner is achieved with the following values for the (normalized) impedances and electrical lengths:

$$\begin{cases} Z_{01} = Z_{02} = Z_{03} = Z_0 \\ Z_{H1} = \sqrt{2} Z_0, & Z_V = Z_0 \\ \theta_{H1} = 90^\circ, & \theta_{H2} = 180^\circ, \quad \theta_V = 90^\circ \end{cases} \quad (1)$$

The last parameter  $Z_{H2}$  is used primarily to control the bandwidth of the combiner. Fig. 2 shows the variation of the coupling bandwidth versus the impedance level for a combiner centered at 4 GHz. For most requirements, a linear circuit simulator can be used to tune the values of the parameters in the ideal circuit for obtaining a performance that satisfies the specifications of a design.

### B. Operation in Both Ideal and Failure Conditions

The circuit shown in Fig. 1(a) can be used as a combiner when two input signals that are both amplitude and phase matched are injected into ports 2 and 3 simultaneously. Then, a combined output signal can be collected at port 1. In ideal

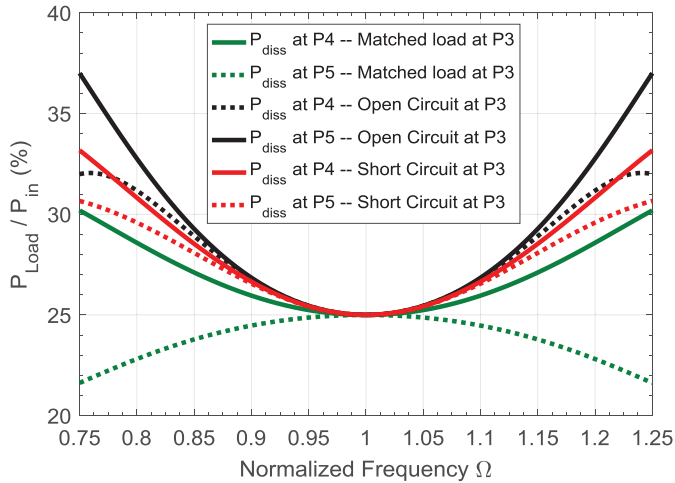


Fig. 3. Power dissipated at the terminations attached to ports 4 and 5 under different loading conditions when input source at P3 fails for the combiner in Fig. 1(a) with  $Z_{01} = Z_{02} = Z_{03} = Z_0$ ,  $Z_{H1} = \sqrt{2}Z_0$ ,  $Z_{H2} = Z_0/\sqrt{2}$ ,  $Z_V = Z_0$ ,  $\theta_{H1} = \theta_{V1} = 90^\circ$ , and  $\theta_{H2} = 180^\circ$ .

operation, at the center frequency of the combiner, no power is delivered to the terminating loads attached to the isolated ports 4 and 5. Suboptimal operation can result due to amplitude mismatch and phase mismatch between input signals.

A limiting case is when one input is completely absent. This can practically take place in situations where power amplifiers fail, presenting a complex load condition at the input port to which they are attached. For example, Fig. 3 presents a case where power  $P_{in}$  is incident at port 2, while a load representing a failed power source is attached to port 3. Power delivered to the terminating loads at ports 4 and 5 is shown for different failure loading conditions at port 3. In essence, at the center frequency, half the input power is delivered to the output, while the other half is split between the two terminating loads. In contrast, for classic designs based on hybrid couplers, half the input power is delivered to a single terminating load.

### III. RIDGE WAVEGUIDE REALIZATION

The realizations of the Gysel combiner proposed in this paper are based on the performance of the circuit scheme shown in Fig. 1(a), with a center frequency of 4 GHz, with parameter values given by (1) and  $Z_{H2} = Z_0/\sqrt{2}$ . This choice secures a 0.5-dB combining loss ( $\sim 90\%$  combining efficiency) over a 41.2% fractional bandwidth and a 1-dB combining loss ( $\sim 80\%$  combining efficiency) over a 52.5% fractional bandwidth.

The designs will implement the transmission lines of the ideal circuit with ridge waveguides arranged in different configurations, providing different alternatives to the system designer in terms of size, port location, and layout. The mapping between the ideal circuit elements and the ridge waveguide sections is shown in Fig. 4. All the input-output ports are ridge waveguides. Later on, subminiature type A (SMA) transitions will be integrated into the design for experimental testing.

The first realization is a design in ridge waveguide, where the sections are arranged in an  $H$ -plane like configuration

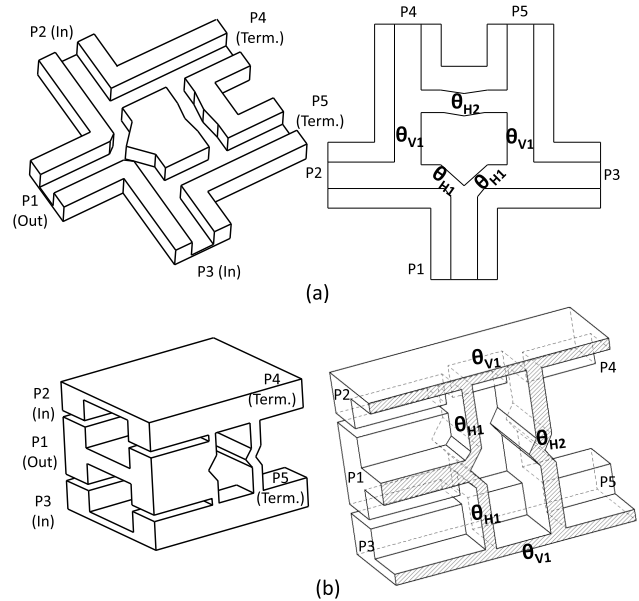


Fig. 4. 3-D models for the waveguide realizations of Gysel combiners with the typical use of the ports and main 2-D views. (a)  $H$ -plane ridge waveguide topology. (b)  $E$ -plane ridge waveguide topology.

along the largest side. Then, a dual realization is given by an  $E$ -plane implementation using ridge waveguides stacked along the height of the ridge waveguide is shown. In the proposed  $E$ -plane design, the port impedances as well as the electrical lengths of the transmission line sections are utilized as additional degrees of freedom in the design process. This enables the realization of compact waveguide combiners. The two designs will target a frequency band of operation extending from 3 to 5 GHz.

#### A. Ridge Waveguide $H$ -Plane Design

The  $H$ -plane design in Fig. 4(a) is suitable for a straightforward synthesis procedure, where clearly identifiable sections of ridge waveguide are associated with a corresponding section in the ideal circuit model. The synthesis requires the calculation of the characteristic impedances and the guided wavelength of ridge waveguide sections. The calculation of the impedance/admittance levels of ridge waveguide sections can start with closed-form expressions [28]. Electromagnetic (EM)-based techniques [29] can also be used to model the discontinuities between sections in order to obtain more refined initial results. For the current design, the dimensions of the waveguide sections are given in Table II according to Fig. 5. The ridge waveguide used at the ports has a fundamental mode with a cutoff frequency of 2.3 GHz, which provides enough margin for the operation centered at 4 GHz.

After synthesizing the ridge waveguide sections, the critical dimensions of the structure are optimized within the 3-D simulation environment to achieve the required performance with respect to the coupling, return loss, and isolation. The optimization follows a classic scheme using an intermediate function with the error for the reflection/isolation given by

$$U(s; g) = \begin{cases} (|s| - |g|)^2, & |s| > |g| \\ 0, & |s| \leq |g| \end{cases} \quad (2)$$

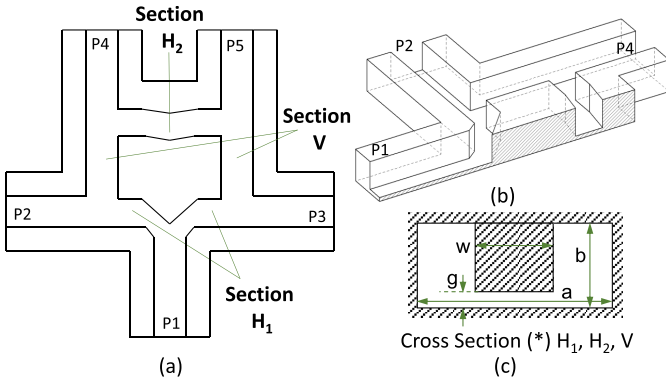


Fig. 5. (a) 2-D view of the  $H$ -plane Gysel combiner. (b) Cut of the structure by the symmetry plane. (c) Cross section of a single-ridge waveguide: (\*) parameters are not necessarily equal in each section.

TABLE II  
DIMENSIONS FOR THE  $H$ -PLANE RIDGE WAVEGUIDE  
GYSEL COMBINER ACCORDING TO FIG. 5

Dimension	Value (mm)	Dimension	Value (mm)
a (all ports)	25.4	b (all ports)	10.16
w (all ports)	10.16	g (all ports)	1.27
g (Section $H_1$ )	1.48	Eq. length sect. $H_1$	19.44
g (Section $H_2$ )	0.54	Eq. length sect. $H_2$	38.46
g (Section $V_1$ )	1.62	Eq. length sect. $V$	20.07

where  $s$  is the S-parameter obtained from the full-wave simulation of the combiner and  $g$  is its corresponding design goal. Then, the cost function is the weighted sum of these errors

$$\begin{aligned}
 f(\mathbf{x}) = & \\
 = & \sum_{i=1}^{N_f} \{ w_{11i} U(S_{11}(f_i, \mathbf{x}); s_{11}^{\text{goal}}) + w_{22i} U(S_{22}(f_i, \mathbf{x}); s_{22}^{\text{goal}}) \\
 & + w_{12i} (|S_{12}(f_i, \mathbf{x})| - |s_{12}^{\text{goal}}|)^2 + w_{14i} U(S_{14}(f_i, \mathbf{x}); s_{14}^{\text{goal}}) \\
 & + w_{23i} U(S_{23}(f_i, \mathbf{x}); s_{23}^{\text{goal}}) \} \quad (3)
 \end{aligned}$$

computed at the selected  $N_f$  frequencies within the band of interest;  $\mathbf{x}$  is the vector with the variables to be optimized and  $w_i$  are the corresponding weights. In order to speed up the full-wave optimization, which can be done for instance using a direct search algorithm, the lengths of the ridge waveguides can be first optimized using just a few frequency points, since the S-parameters of the combiner have a smooth variation.

The optimized results for the combiner are shown in Fig. 6. They have been calculated using Ansys HFSS. An ideal case combining loss better than 1 dB is obtained over a 50% fractional bandwidth. This is possible due to the inherent characteristics of ridge waveguide, where the single-mode bandwidth is much wider than that of rectangular waveguides. (The cutoff frequency of the first higher order mode is 10.9 GHz for the selected ridge waveguide.) This is in addition to the size reduction with respect to a rectangular waveguide having the same cutoff frequency for the fundamental mode, which would require a width of 64.4 mm. Here, the bandwidth is referenced to the combining loss rather than return loss or

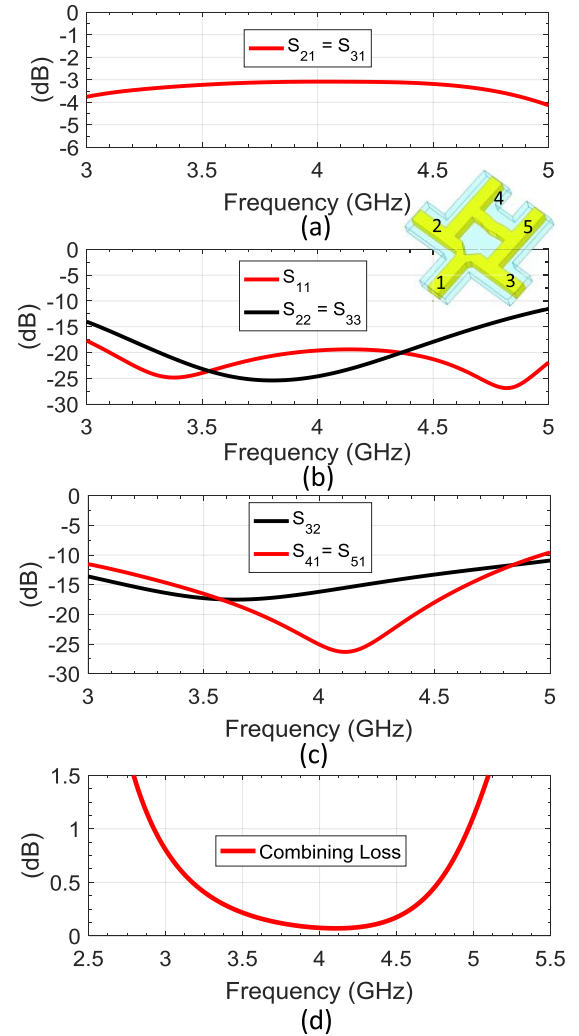


Fig. 6. Simulated results of the  $H$ -plane ridge waveguide Gysel combiner. (a) Coupling. (b) Return loss. (c) Isolation. (d) Combining loss.

isolation (classical case in standalone couplers), since the intended use of the structure is power combination, where combining loss and, hence, efficiency are the most important attribute.

### B. Ridge Waveguide E-Plane Design

The  $E$ -plane ridge waveguide topology is shown in Fig. 4(b), with ridge waveguide sections arranged in a stacked top-to-bottom configuration. Single-ridge waveguide sections realize the input as well as the isolated ports. However, the output port is a double-ridge waveguide to preserve and utilize the symmetry of the structure. Due to the symmetry of the combiner along the plane passing through the middle of its gap region, double-ridge waveguide will have the same cutoff frequency of the fundamental mode of a single-ridge waveguide obtained by inserting an electric wall at that symmetry plane. Nevertheless, the double-ridge waveguide provides higher power handling capability, since it has double the physical gap of the corresponding single-ridge waveguide. This approach provides an opportunity to increase the power handling capability of the combiner in comparison to the

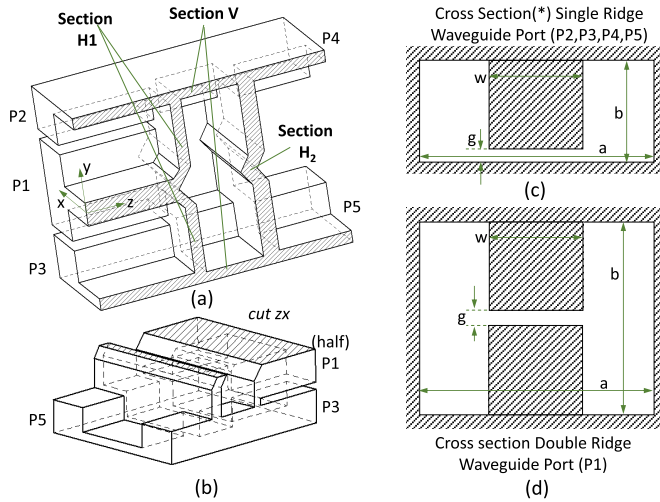


Fig. 7. (a) and (b) Cuts of the  $E$ -plane combiner by the symmetry  $yz$  and  $zx$  planes (c) and (d) with the involved ridge waveguides in the ports: (\*) parameters are not necessarily equal in each port.

TABLE III  
DIMENSIONS FOR THE  $E$ -PLANE RIDGE WAVEGUIDE  
GYSEL COMBINER ACCORDING TO FIG. 7

Dimension	Value (mm)	Dimension	Value (mm)
a (P1)	55.4	b (P1)	22.86
w (P1)	27.94	g (P1)	6.1
a (P2, P3)	55.4	b (P2,P3)	11.43
w (P2,P3)	27.94	g (P2,P3)	3.6
a (P4, P5)	55.4	b (P4, P5)	11.43
w (P4, P5)	27.94	g (P4, P5)	2.4
g (Section $H_1$ )	3.29	Eq. length sect. $H_1$	23.8
g (Section $H_2$ )	3.94	Eq. length sect. $H_2$	46.86
g (Section $V$ )	2.78	Eq. length sect. $V$	15.14

$H$ -plane configuration, since the output port, which carries the combined power, can handle now more power by the virtue of its larger gap.

The calculation of the impedance/admittance levels of ridge waveguide sections can be done in a similar fashion to the  $H$ -plane case. In this particular design, after the initial synthesis, and during optimization, the port impedance levels are used as additional degrees of freedom. Thus, the input and isolated ports are allowed to have impedance values other than that of the output port.

The dimensions of the waveguide sections are given in Table III according to Fig. 7. Nevertheless, it is worth noting that the realization for section  $H_1$ , and in particular  $H_2$ , when looking from the top/bottom of the structure (along the  $y$ -axis) is now composed of a set of double-ridge waveguide with a rectangular waveguide section in between them. The discontinuity effects are accounted for in the EM model, since a final full-wave optimization of this structure is used to obtain the required response.

The optimized results for the combiner using ridge waveguide ports are shown in Fig. 8. An ideal case of a combining loss better than 1 dB is obtained over a 53%

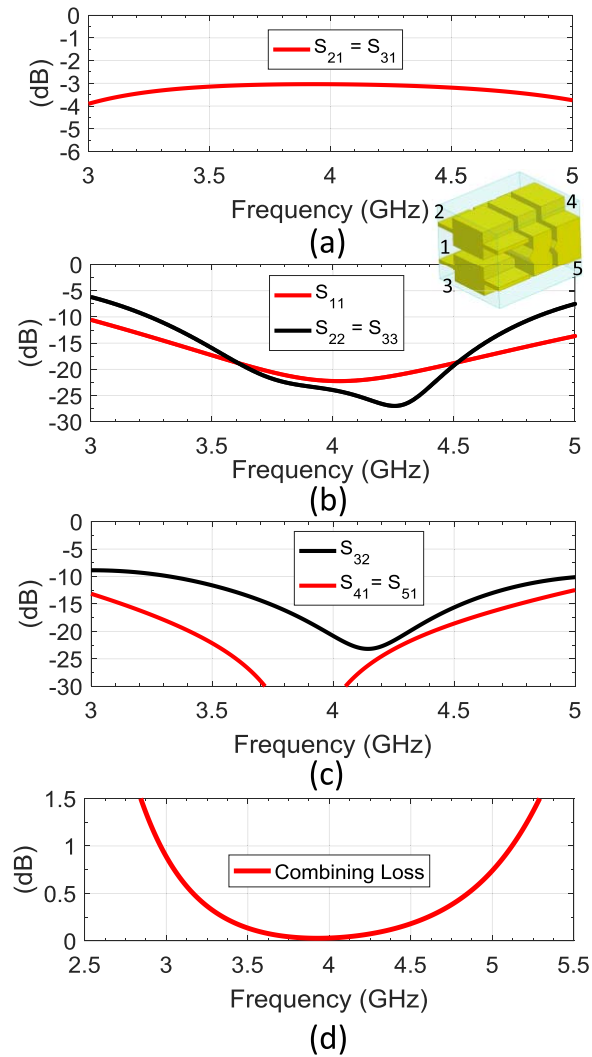


Fig. 8. Simulated results of the  $E$ -plane ridge waveguide Gysel combiner. (a) Coupling. (b) Return loss. (c) Isolation. (d) Combining loss.

fractional bandwidth, as shown in Fig. 8(d), with a combining loss of 0.5 dB obtained over a 42% fractional bandwidth.

#### IV. EXPERIMENTAL RESULTS

The two designs were manufactured and tested. The Gysel combiners were designed with ridge waveguide ports in previous sections. However, in order to facilitate measurements of the prototype, transitions to SMA coaxial transmission lines were needed. In addition, for an eventual ultimate integration of the combiners in systems where power from the input devices need to be launched into the combiner using coaxial ports, these transitions were integrated in the combiner (not as separate parts, but included in the same hardware). The designs were fabricated out of aluminum by computer numerical controlled milling. No tuning was required for the prototypes. The hardware units were not plated in these proofs of concept designs. Certainly, silver plating of the units can improve their loss performance.

##### A. Implementation of the Ridge Waveguide $H$ -Plane Design

For the  $H$ -plane design, a wideband SMA to single-ridge waveguide transition (that will be referred to as T1) was

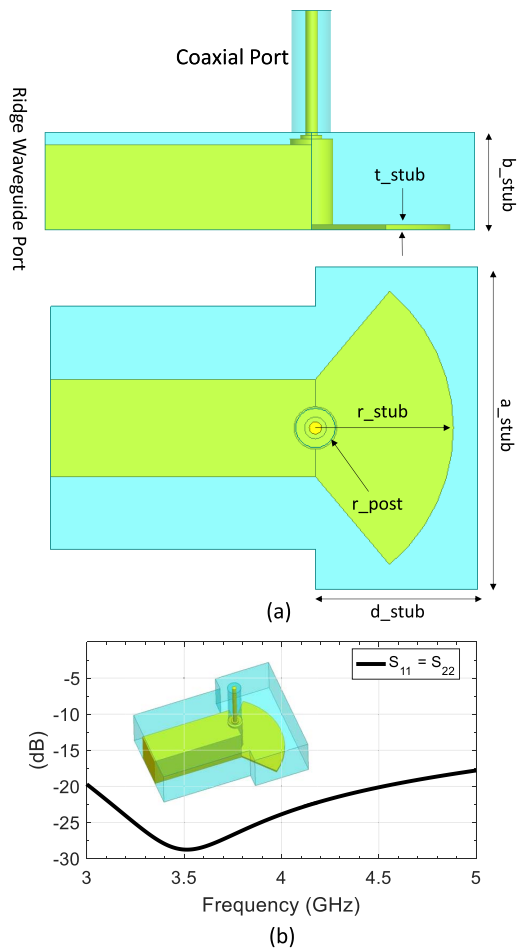


Fig. 9. Transition T1 from single-ridge waveguide to SMA coaxial line. (a) Layout. (b) Return loss.

TABLE IV

DIMENSIONS OF TRANSITION T1 FROM SINGLE-RIDGE WAVEGUIDE PORT IN THE  $H$ -PLANE DESIGN TO SMA COAXIAL LINE AS IN FIG. 9

Dimension	Value (mm)	Dimension	Value (mm)
a_stub	33.68	b_stub	10.16
d_stub	16.94	r_stub	12.17
t_stub	0.51	r_post	2.23

designed separately. The design followed the methodology detailed in [30], with a radial stub section shown in Fig. 9(a). Then, the five identical transitions were attached to the ridge waveguide ports of the  $H$ -plane combiner. The standalone transition and its full-wave response are shown in Fig. 9(b), while its dimensions are given in Table IV.

The  $H$ -plane ridge waveguide design was manufactured out of a housing with integrated transitions to SMA and a cover that has holes for inserting the SMA launchers. The combiner with all its transitions is shown in Fig. 10(a). Without the wall thickness, it occupies a volume of merely 120 mm  $\times$  113 mm  $\times$  10 mm, a very compact design for the C-band frequency band of interest. A photograph of the housing is shown in Fig. 10(b), while the measured results are shown in Fig. 11.

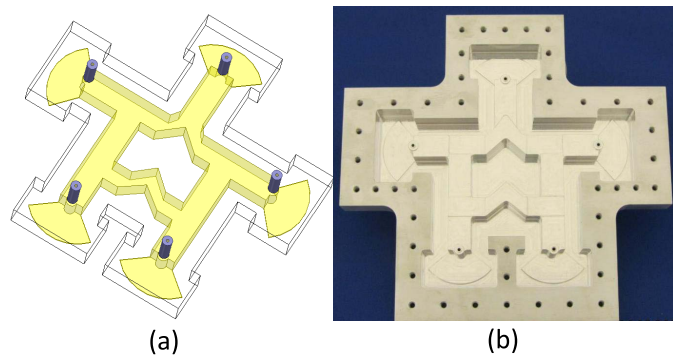


Fig. 10. (a)  $H$ -plane ridge waveguide Gysel combiner with the integrated coaxial transitions. (b) Manufactured unit without cover.

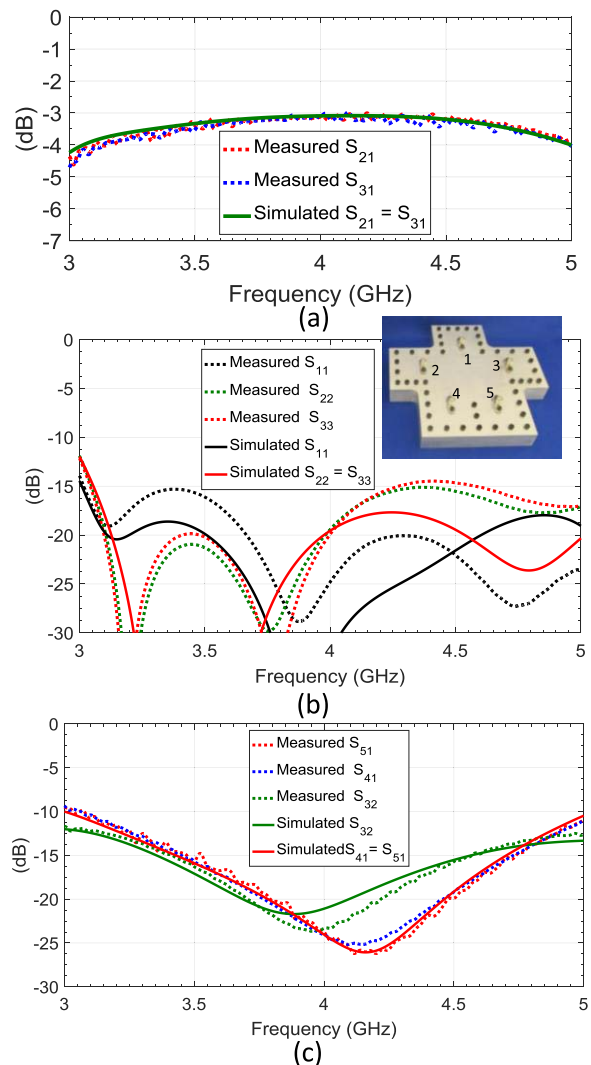


Fig. 11. Measured and full-wave simulated results of the  $H$ -plane ridge waveguide Gysel combiner in Fig. 10. (a) Coupling. (b) Return loss. (c) Isolation.

It can be seen in Fig. 11 that the experimental results agree well with the full-wave simulated results. No tuning elements were incorporated into the hardware to get these experimental results.

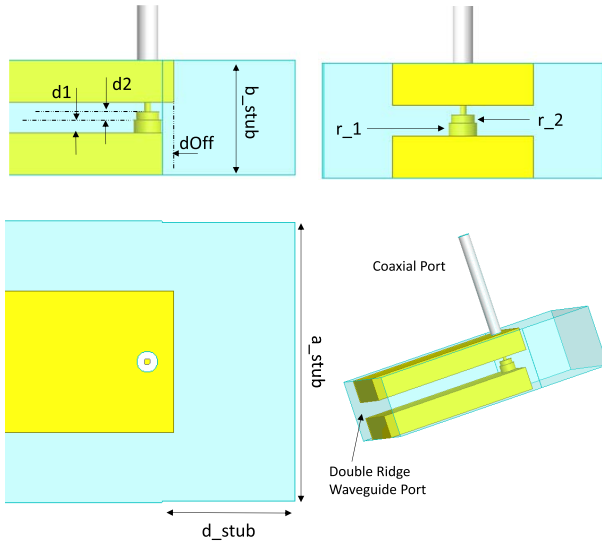


Fig. 12. Layout of transition T4 from double-ridge waveguide to SMA coaxial line.

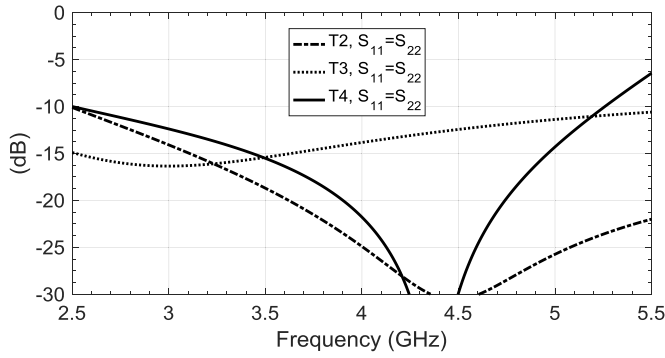


Fig. 13. Return loss for transitions T2 and T3 (between single-ridge waveguide for ports 2, 3 and 4, 5, respectively, and SMA), and T4 (between double-ridge waveguide at port 1 and SMA).

### B. Implementation of the Ridge Waveguide E-Plane Design

In this case, three different transitions (T2, T3, and T4) were needed to facilitate the measurements and future system integration of the combiner. The transitions are between single- and double-ridge waveguide sections and SMA coaxial lines. These transitions were designed keeping in mind their mechanical integration with the *E*-plane combiner.

Transition T2 was designed for ports 2 and 3, while transition T3 was designed for ports 4 and 5. Both transitions have layouts similar to transition T1 shown in Fig. 9(a). Transition T4 from double-ridge waveguide to SMA was designed and integrated into port 1. Fig. 12 shows the layout of transition T4.

All these stand-alone transitions were optimized to operate in the same frequency band as the combiner. Upon integration with the combiner slight adjustments are needed to take into account the finite return loss at their respective planes of interconnection with the combiner, which results in small changes in the overall return loss and isolation of the combiner.

The dimensions are given in Tables V and VI. Fig. 13 shows the response of T2, T3, and T4, each satisfying the requirements of the ports to which they are attached.

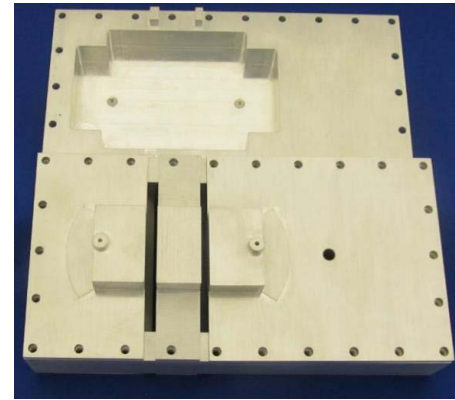
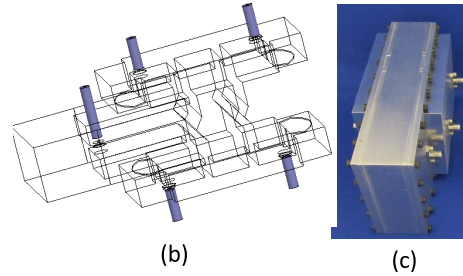
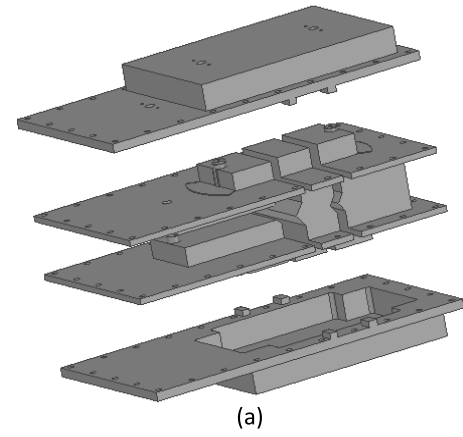


Fig. 14. (a) CAD model of the mechanical assembly for the *E*-plane ridge waveguide combiner. (b) 3-D EM model for full-wave simulation. (c) Assembled manufactured combiner. (d) Combiner with the last part acting as cover open.

TABLE V  
DIMENSIONS OF TRANSITIONS [T2, T3] FROM SINGLE-RIDGE WAVEGUIDES TO SMA COAXIAL LINE AS IN FIG. 9

Dimension	Value (mm)	Dimension	Value (mm)
a stub	[39.46,39.58]	b stub	[11.43,11.43]
d stub	[12.59,12.69]	r stub	[9.63,9.73]
t stub	[0.34,0.34]	r post	[2.89,2.89]

The final waveguide structure has waveguide sections with different longitudinal axes and its manufacturing involves the integration of several parts, as shown in Fig. 14. The combiner was manufactured out of an assembly, comprising a housing and multiple inserts. Fig. 14(a) shows an exploded view representing how different mechanical parts are assembled to realize the combiner, where the different metallic parts realize the ridge waveguide sections once they are integrated.

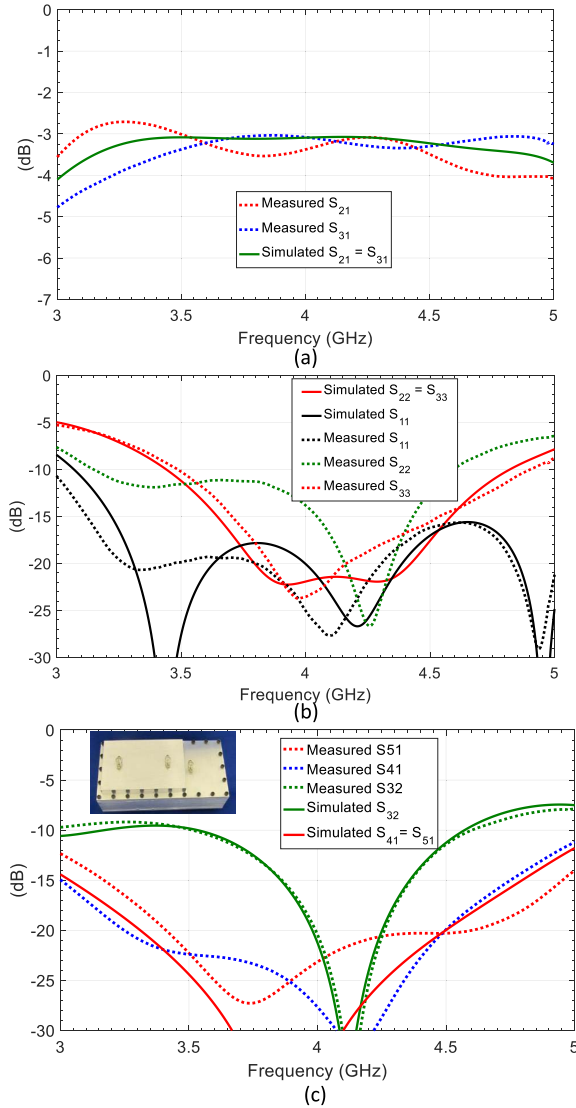


Fig. 15. Measured and full-wave simulated results of the *E*-plane ridge waveguide Gysel combiner in Fig. 14. (a) Coupling. (b) Return loss. (c) Isolation.

TABLE VI

DIMENSIONS OF TRANSITION T4 FROM DOUBLE-RIDGE WAVEGUIDE TO SMA COAXIAL LINE AS IN FIG. 12.

Dimension	Value (mm)	Dimension	Value (mm)
a stub	55.32	b stub	22.86
d stub	26.35	dOff	2.38
[r1, r2]	[2.8, 2.29]	[d1, d2]	[2.62, 1.6]

Moreover, the transitions to SMA ports are also integrated in the same structure, as shown in the EM model in Fig. 14(b). This EM model fits in a volume of 56 mm × 51 mm × 116 mm. A photograph of the fully assembled combiner with its coaxial ports on one side is shown in Fig. 14(c). The partial assembly of the combiner, before the last part is used to close the structure, is shown in Fig. 14(d). Fig. 14(d) also shows the holes for the SMA coaxial launchers that will be attached to the housing.

The experimental results for the main S-parameters of the combiner are shown in Fig. 15. The measured results agree

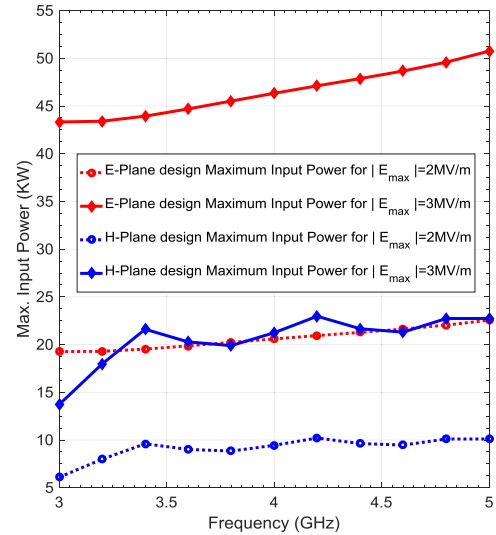


Fig. 16. Maximum input power analysis for the ridge waveguide *E*-plane and *H*-plane Gysel combiners.

well with the simulated results, except for some degradation of the return loss at port 2, due to mechanical misalignment at this port during the final assembly.

It is important to note that for the *E*-plane topology the inputs have to be 180° out of phase for the combiner to work properly, in contrast with the *H*-plane topology, where they have to be in-phase. This is due to the field distribution in the *E*-plane bifurcation as compared to the *H*-plane bifurcation.

### C. Power Handling Comparison

The theoretical EM analysis of maximum power handling in the two designed structures is shown in Fig. 16. First, the maximum electric field intensity within the structure is calculated using EM field solvers [30] for a certain input power level. By using proportionality relations, estimates of the power levels that will correspond to certain electric field intensities can be calculated. The theoretical limit for breakdown in air is of 3 MV/m. A maximum allowed electric field strength of 2 MV/m is assumed in the calculation of the power rating to have a safety margin with respect to the theoretical limit. Both structures can handle input power in the multi-kilowatt range; however, the *E*-plane design, understandably, offers better power handling capabilities.

## V. CONCLUSION

Two novel ridge waveguide realizations of Gysel combiners were presented. Gysel combiners offer better bandwidth and require terminating loads with half the ratings in comparison to conventional combiners. Two types of designs have been proposed for exploiting these advantages in ridge waveguide. A comprehensive treatment of the realization of the combiners has been discussed, where variation of port impedance and electrical length of combiner sections is used to provide additional needed degrees of freedom to the designer to enable the realization of the performance within a compact overall size. Finally, two experimental prototypes were manufactured with

different assembly strategies. Test results of the prototype units show good agreement with theoretical predictions, validating the designs for promising high-power combining wideband applications.

#### ACKNOWLEDGMENT

This work was performed under the auspices of the University of Waterloo. The authors would like to thank A. Fouladi from the Centre for Integrated RF Engineering, University of Waterloo, Waterloo, ON, Canada, for help with logistics and measurements.

#### REFERENCES

- [1] K. J. Russell, "Microwave power combining techniques," *IEEE Trans. Microw. Theory Techn.*, vol. MTT-27, no. 5, pp. 472–478, May 1979.
- [2] K. Chang and C. Sun, "Millimeter-wave power-combining techniques," *IEEE Trans. Microw. Theory Techn.*, vol. MTT-31, no. 2, pp. 91–107, Feb. 1983.
- [3] J. C. Freeman, E. G. Wintucky, and C. T. Chevalier, "High power high efficiency Ka-band power combiners for solid-state devices," NASA, Washington, DC, USA, Tech. Rep. NASA/TM-2006-214447, 2006.
- [4] K. R. Vaden, "Computer aided design of Ka-band waveguide power combining architectures for interplanetary spacecraft," NASA, Washington, DC, USA, Tech. Rep. NASA/TM-2006-214108, 2006, pp. 1–7.
- [5] R. N. Simons, E. G. Wintucky, J. D. Wilson, and D. A. Force, "Ultra-high power and efficiency space TWTA power combiner with reduced size and mass for NASA missions," *IEEE Trans. Microw. Theory Techn.*, vol. 57, no. 3, pp. 582–588, Mar. 2009.
- [6] Q. Xue, K. Song, and C. H. Chan, "China: Power combiners/dividers," *IEEE Microw. Mag.*, vol. 12, no. 3, pp. 96–106, May 2011.
- [7] S.-W. Dong, Y.-Z. Dong, Y. Wang, and L.-M. Gong, "High power and efficiency power combining with multi-way TWTAs for satellite communications," in *IEEE MTT-S Int. Microw. Symp. Dig.*, Jun. 2012, pp. 1–3.
- [8] K. Song, F. Zhang, S. Hu, and Y. Fan, "Ku-band 200-W pulsed power amplifier based on waveguide spatially power-combining technique for industrial applications," *IEEE Trans. Ind. Electron.*, vol. 61, no. 8, pp. 4274–4280, Aug. 2014.
- [9] L. T. Guo *et al.*, "Design of compact high-isolation four-way power combiners," *IEEE Trans. Microw. Theory Techn.*, vol. 66, no. 5, pp. 2185–2198, May 2018.
- [10] S. B. Erekson, W. J. D. Johnson, and D. Peroulis, "Design of an airline coax radial power combiner with enhanced isolation," in *IEEE MTT-S Int. Microw. Symp. Dig.*, Honolulu, HI, USA, Jun. 2017, pp. 455–458.
- [11] R. Kazemi, G. Hegazi, and A. E. Fathy, "X-band all-waveguide radial combiner for high power applications," in *IEEE MTT-S Int. Microw. Symp. Dig.*, Phoenix, AZ, USA, May 2015, pp. 1–4.
- [12] H. Theveneau, C. Gaquière, R. Lenglet, M. Werquin, J.-C. Joly, and S. Torte, "Spatial power combiner with low-impedance inputs and increased isolation," *IEEE Microw. Wireless Compon. Lett.*, vol. 27, no. 11, pp. 956–958, Nov. 2017.
- [13] J. R. Montejo-Garai, I. O. Saracho-Pantoja, J. A. Ruiz-Cruz, and J. M. Rebolgar, "High-performance 16-way Ku-band radial power combiner based on the TE<sub>01</sub>-circular waveguide mode," *Rev. Sci. Instrum.*, vol. 89, no. 3, p. 034703, 2018.
- [14] Q.-X. Chu, D.-Y. Mo, and Q.-S. Wu, "An isolated radial power divider via circular waveguide TE<sub>01</sub>-mode transducer," *IEEE Trans. Microw. Theory Techn.*, vol. 63, no. 12, pp. 3988–3996, Dec. 2015.
- [15] A. Buesa-Zubiria and J. Esteban, "Design of five-way Bagley polygon power dividers in rectangular waveguide," *IEEE Trans. Microw. Theory Techn.*, vol. 66, no. 1, pp. 116–127, Jan. 2018.
- [16] J. Bornemann, U. Rosenberg, S. Amari, and S. S. Hesari, "Design of sum-difference power combiners with second-order filtering functions," in *IEEE MTT-S Int. Microw. Symp. Dig.*, Seville, Spain, May 2017, pp. 296–298.
- [17] X. Shan and Z. Shen, "An eight-way power combiner based on a transition between rectangular waveguide and multiple microstrip lines," *IEEE Trans. Microw. Theory Techn.*, vol. 61, no. 7, pp. 2585–2593, Jul. 2013.
- [18] U. H. Gysel, "A new N-way power divider/combiner suitable for high-power applications," in *IEEE MTT-S Int. Microw. Symp. Dig.*, Palo Alto, CA, USA, May 1975, pp. 116–118.
- [19] L.-S. Wu, Y.-X. Guo, and J.-F. Mao, "Balanced-to-balanced Gysel power divider with bandpass filtering response," *IEEE Trans. Microw. Theory Techn.*, vol. 61, no. 12, pp. 4052–4062, Dec. 2013.
- [20] Y. Wu, Y. Liu, and S. Li, "A modified Gysel power divider of arbitrary power ratio and real terminated impedances," *IEEE Microw. Wireless Compon. Lett.*, vol. 21, no. 11, pp. 601–603, Nov. 2011.
- [21] F. Lin, Q.-X. Chu, Z. Gong, and Z. Lin, "Compact broadband Gysel power divider with arbitrary power-dividing ratio using microstrip/slotline phase inverter," *IEEE Trans. Microw. Theory Techn.*, vol. 60, no. 5, pp. 1226–1234, May 2012.
- [22] K. X. Wang, X. Y. Zhang, and B.-J. Hu, "Gysel power divider with arbitrary power ratios and filtering responses using coupling structure," *IEEE Trans. Microw. Theory Techn.*, vol. 62, no. 3, pp. 431–440, Mar. 2014.
- [23] H. S. Gharehaghaji and H. Shamsi, "Design of unequal dual band Gysel power divider with isolation bandwidth improvement," *IEEE Microw. Wireless Compon. Lett.*, vol. 27, no. 2, pp. 138–140, Feb. 2017.
- [24] H. Chen, W. Che, C. Gu, and W. Feng, "A novel Gysel power divider based on substrate-integrated-waveguide (SIW) technology," in *Proc. Eur. Microw. Conf.*, Paris, France, Sep. 2015, pp. 1–4.
- [25] H. Chen, W. Che, X. Wang, and W. Feng, "Size-reduced planar and nonplanar SIW Gysel power divider based on low temperature co-fired ceramic technology," *IEEE Microw. Wireless Compon. Lett.*, vol. 27, no. 12, pp. 1065–1067, Dec. 2017.
- [26] M. M. Fahmi and R. R. Mansour, "Compact ridge waveguide Gysel combiner," in *IEEE MTT-S Int. Microw. Symp. Dig.*, Philadelphia, PA, USA, Jun. 2018, pp. 9–11.
- [27] A. Grebennikov, "Power combiners, impedance transformers and directional couplers: Part II," *High Freq. Electron.*, vol. 7, pp. 42–53 Jan. 2008.
- [28] W. J. R. Hoefler and M. N. Burton, "Closed-form expressions for the parameters of finned and ridged waveguides," *IEEE Trans. Microw. Theory Techn.*, vol. MTT-30, no. 12, pp. 2190–2194, Dec. 1982.
- [29] M. M. Fahmi, J. A. Ruiz-Cruz, and K. A. Zaki, "E and H-plane wide-band ridge waveguide couplers," *Int. J. RF Microw. Comput.-Aided Eng.*, vol. 18, no. 4, pp. 348–358, 2008.
- [30] S. B. Cohn, "Design of simple broad-band wave-guide-to-coaxial-line junctions," *Proc. IRE*, vol. 35, no. 9, pp. 920–926, Sep. 1947.



**Mohamed M. Fahmi** received the B.Sc. degree (Hons.) in electronics engineering from Mansoura University, Mansoura, Egypt, in 1999, the M.S. degree in electrical engineering from Howard University, Washington, DC, USA, in 2003, and the Ph.D. degree in electrical engineering from the University of Maryland, College Park, MD, USA, in 2007.

In 2008, he joined the Department of Electrical and Computer Engineering, University of Maryland, as a Post-Doctoral Researcher. From 2008 to 2012, he was a Post-Doctoral Fellow with the Department of Electrical and Computer Engineering, University of Waterloo, Waterloo, ON, Canada. From 2012 to 2017, he was a Microwave Engineer, a Senior Microwave Engineer, and a Manager of Passive Component Engineering with Nanowave Technologies Inc., Etobicoke, ON, Canada. From 2017 to 2018, he was a Senior System Engineer and a Radar Specialist with General Dynamics Mission Systems Canada, Ottawa, ON, Canada. In 2018, he joined Defence Research and Development Canada, Ottawa, as a Group Leader of Radar Technology and Engineering. He is also an Adjunct Assistant Professor with the Department of Electrical and Computer Engineering, University of Waterloo. His current research interests include computer-aided design of microwave devices and systems.



**Jorge A. Ruiz-Cruz** (SM'11) received the Ingeniero de Telecomunicación and Ph.D. degrees from the Universidad Politécnica de Madrid, Madrid, Spain, in 1999 and 2005, respectively.

Since 2006, he has been with the Universidad Autónoma de Madrid, Madrid, where he became an Associate Professor in 2009. His current research interests include computer-aided design of microwave passive devices and circuits (filters, multiplexers, and ortho-modes).



**Raafat R. Mansour** (S'84–M'86–SM'90–F'01) received the B.Sc. (with honors) and M.Sc. degrees in electrical engineering from Ain Shams University, Cairo, Egypt, in 1977 and 1981, respectively, and the Ph.D. degree in electrical engineering from the University of Waterloo, Waterloo, ON, Canada, in 1986.

Over the period 1986–1999 he was with COM DEV Ltd., Cambridge, ON, Canada, where he held several technical and management positions with the company Corporate Research and Development Department. Since January 2000, he has been a Professor with the Electrical and Computer Engineering Department, University of Waterloo, where he was a Natural Sciences and Engineering Research Council of Canada (NSERC) Industrial Research Chair from 2001 to 2010. He currently holds a Tier I Canada Research Chair. He is the Founding Director of the Centre for Integrated RF Engineering. He has authored or co-authored numerous publications in the areas of filters and multiplexers, superconductivity, and microelectromechanical systems (MEMS). He co-authored a Wiley book and contributed six chapters to other four books. He holds several patents related to the areas of dielectric resonator filters, superconductivity, and MEMS devices. His current research interests include MEMS and PCM technologies and tunable microwave and millimeter-wave devices.

Dr. Mansour is a Fellow of the Engineering Institute of Canada (EIC) and of the Canadian Academy of Engineering (CAE). He was a recipient of COM DEV's Outstanding Achievement Award in 1991, COM DEV's CEO Award in 1994, several Best Paper Awards, Outstanding Research Performance Awards from the University of Waterloo, and the 2014 Professional Engineers Ontario (PEO) Engineering Medal for Research and Development.